Available online at www.sciencedirect.com
SCIENCE DIRECT®
International Journal of Thermal Sciences 42 (2003) 255–265
International Journal of Thermal Sciences
www.elsevier.com/locate/ijts

Experimental modelling and estimation of time varying thermal sources

Etienne Videcoq [a,*], Daniel Petit [b], André Piteau [b]

[a] *I.U.T. génie thermique et énergie, chemin de la Tuilerie, 91731 Bretigny sur Orge, France*
[b] *Laboratoire d'études thermiques, U.M.R. 6608, E.N.S.M.A., B.P. 109 86960 Futuroscope cedex, France*

Received 21 July 2001; accepted 28 May 2002

Abstract

This paper shows an experimental design where two steps are carried out: (i) the identification of a low order state representation through temperature evolutions corresponding to step responses of a system, (ii) the use of this model to solve an inverse heat conduction problem (IHCP) consisting in the estimation of several strength variations generated by heat sources from time-varying temperature evolutions.

Experiments are realized on a 3D heat conductive system (a thick stainless steel tube) in which are set four heat sources, a fifth thermal strength consists in an applied flux boundary condition. After the model identification, a sequential method is used for the resolution of the IHCP: from temperature measurements, the evolutions of the five strengths are identified and compared to the electrical measurements.

Keywords: 3D heat conduction; Inverse problem; Experiment; Linear system; Dominant eigenmodes; Experimental modelling; Heat source strength estimation; Function specification; Future time steps; Multi-input multi-output

1. Introduction

As a general rule, an inverse heat conduction problem (IHCP) consists in the estimation of physical parameters, initial conditions, boundary conditions or heat sources from temperature measurements [1–3]. For multi-dimensional heat conduction problems, a fine description of the studied system by a classical modelling (finite elements, control volumes, ...) leads to a model of high dimension which becomes much more difficult to use with experimental or simulated data [4,5]. In order to lighten this drawback, techniques using the boundary elements [6,7] or the discrete cosine transform analysis [8] can be used.

The results of the IHCP depend strongly on the accuracy of the modelling: all the parameters that are supposed to be known (boundary conditions, thermal properties, thermal resistances, etc.) must be well evaluated before the inversion.

Due to the ill-posed nature of the inverse problem, the time varying estimation of the heat source intensities is highly sensitive to sensor position. In order to regularize the IHCP, the function specification method due to Beck [1,9, 10] can be used.

In order to avoid difficulties in relation to high-dimensional model and in relation with a good knowledge of all the previous parameters, we use here an Identified Model (IM) which is obtained from some specific experiments. Then, by using this IM—which is low dimensioned—we propose to estimate five time varying unknowns from the knowledge of temperature evolutions at some points of the domain. In this field of investigation, previous numerical works have already been presented concerning the resolution of IHCP through a reduced model [11,12].

The originality of this work consists in an experimental application of the methodology, using a three-dimensional diffusive medium, in which are located heat sources and thermocouples. The objective is to estimate simultaneously four unknown heat source strengths and one boundary condition (heat flux). The method used to build IM uses only decreasing temperature measurements. This experimental modelling, based on responses to step inputs, does not require the knowledge of the thermal properties and constitutes then a calibration tool, which then allows solving the IHCP.

In the first part of the paper, the experimental device is described. Then, the principles of the model identification method are presented. Afterwards, the inverse method is developed through the use of future time. Finally, some

* Corresponding author.
E-mail addresses: e.videcoq@iut.univ-evry.fr (E. Videcoq), daniel.petit@let.ensma.fr (D. Petit).

1290-0729/02/$ – see front matter
doi:10.1016/S1290-0729(02)00025-X

Nomenclature

c_P	specific heat	$J{\cdot}kg^{-1}{\cdot}K^{-1}$
$\boldsymbol{f}(m,m)$	diagonal matrix relative to current EIM	s^{-1}
$\boldsymbol{F}(n,n)$	diagonal matrix of eigenvalues for IM	s^{-1}
$\boldsymbol{g}(m)$	vector applying $\dot{u}$	
$\boldsymbol{G}(n,p)$	input matrix for IM	
$\boldsymbol{h}(q,m)$	output matrix relative to current EIM	
$\boldsymbol{H}(q,n)$	output matrix for IM	
m	order of EIM	
n	order of IM	
nf	number of future times for specification function	
nt	number of measurement times	
p	dimension of input vector	
q	number of sensors	
q_V	volume heat source	$W{\cdot}m^{-3}$
R	electric resistance	Ω
$\boldsymbol{s}(q)$	static vector relative to current EIM	
$\boldsymbol{S}(q,p)$	static matrix, static sensitivity matrix	
$S_{i,j}$	static sensitivity of sensor i relatively to input j	
$\boldsymbol{T}, \dot{\boldsymbol{T}}$	temperature vector, its derivative	K, $K{\cdot}s^{-1}$
$u, \dot{u}$	current component of U, its derivative	
$\boldsymbol{U}(p)$	input vector	
$\boldsymbol{x}, \dot{\boldsymbol{x}}(m)$	EIM state vector, its derivative	
$\boldsymbol{y}(q)$	EIM output vector	
$\boldsymbol{Y}(q)$	output vector for IM	K
$\boldsymbol{Z}$	macro output vector	K

Abbreviations

DM	Detailed Model
EIM	Elementary Identified Model
FTS	Future Time Step
IHCP	Inverse Heat Conduction Problem
IM	Identified Model

Greeks symbols

Δt	time step	s
λ	thermal conductivity	$W{\cdot}m^{-1}{\cdot}K^{-1}$
ρ	density	$kg{\cdot}m^{-3}$
σ_Y	root mean square for $\boldsymbol{Y}$	K
τ	time constant	s

Superscripts

T	transposition sign
*	measured value

results presenting the estimation of the five heat source strengths are compared to the electrical measurements.

2. Experimental device and process

The main part of the experiment is a thick cylinder (external diameter = 100 mm, internal diameter = 20 mm, length = 150 mm) composed of stainless steel whose properties are $\lambda = 14.9\ W{\cdot}m^{-1}{\cdot}{}^{\circ}C^{-1}$, $c_P = 477\ J{\cdot}kg^{-1}{\cdot}{}^{\circ}C^{-1}$ and $\rho = 7900\ kg{\cdot}m^{-3}$. The external surface of this cylinder is insulated with rock wool (100 mm thick). Five heat sources and twenty T-type thermocouples in a stainless steel sheath (3 mm in external diameter and 30 mm long) are placed in different sections and depths of the device. A general view of the position of the sources and thermocouples is given in Fig. 1. Four cylindrical heat elements (6.5 mm in diameter and 40 mm long) represent 4 volume sources: VS1, VS2, VS3 and VS4. The fifth heat source is a surface source SS5. It is a heater ring placed on the external surface of the stainless steel cylinder.

Note that an optimal position has not been chosen for the sensors. The aim here was to set several sensors in the wall tube and then to solve the IHCP with different configurations, including the optimum one.

Fig. 2 shows a general view of the device. The sources are driven through a five-channel power modulator. By removing periods of the main supply, each channel can be adjusted from 1% to 100% of the maximum power of the thermal heating. The dissipated power in each source depends on the supply voltage and the mean resistance of each element. Table 1 shows the mean value of each resistance. The temperature dependence of the resistance is low for our power domain. The power modulator is controlled from the PC, as well as the timing of the power modulation. The strength of each heat source is then calculated with the voltage and the resistance R of the heating device.

The heat extraction is realised with a high-rate water flow that maintains a constant temperature in a closed circuit with a refrigerated circulator, in such a way that the temperature difference between the inlet and the outlet is small (about 0.2 °C maximum). The heat transfer coefficient between the solid and the water is supposed to be constant because the flow rate does not vary in time. The temperature measurements in the cylinder and water flow are given by thermocouples connected to the data acquisition system.

In order to decrease the measurement noise of the thermocouples, each acquisition corresponds to a mean between four temperatures recorded successively at 20 Hz. These measurements are stored in the PC for future calculation.

Table 1
Mean electric resistance of each heat source

	VS1	VS2	VS3	VS4	SS5
R(Ω)	430	421	455	418	89

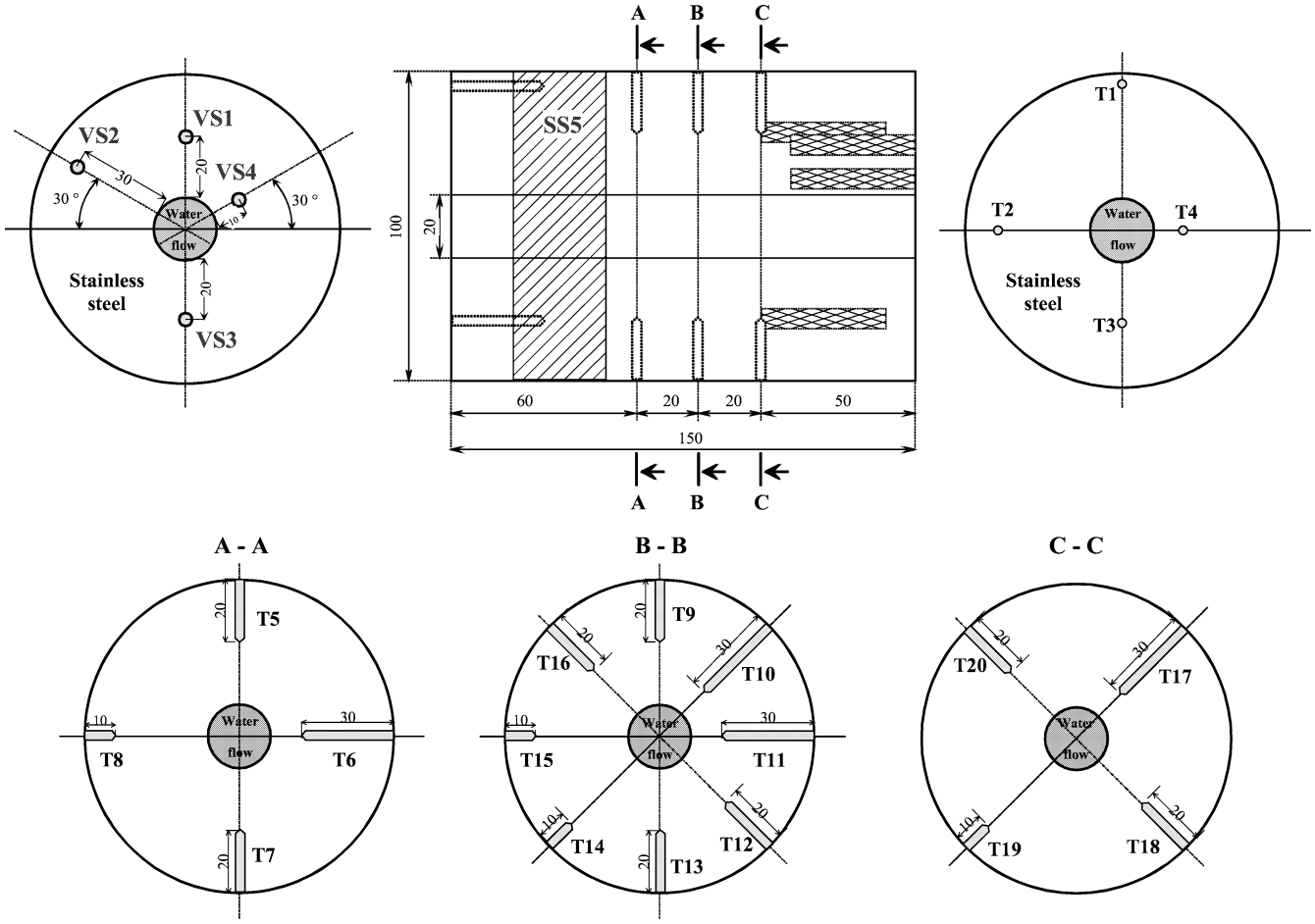

Fig. 1. The 3D diffusive system. Position of the 5 heat sources and the 20 thermocouples (dimensions in mm).

3. The identified model

3.1. Model structure

Heat transfer inside the thick cylinder is governed by the energy equation:

$$\rho \cdot c_P \cdot \frac{\partial T}{\partial t} = \lambda \cdot \nabla^2 T + q_V \tag{1}$$

associated to initial and boundary conditions. In Eq. (1), λ, ρ and c_P are the material properties, T the temperature, t the time and q_V the volume source term. Classically, in order to identify the heat sources, a 3D spatial discretization is necessary through a finite element method for example.

In previous works [11–14], it has been shown how the discretization of Eq. (1) could be written under a state-space formulation called Detailed Model (DM):

$$\begin{cases} \dot{\boldsymbol{T}}(t) = \boldsymbol{A}\boldsymbol{T}(t) + \boldsymbol{B}\boldsymbol{U}(t) & \text{(a)} \\ \boldsymbol{Y}(t) = \boldsymbol{D}\boldsymbol{T}(t) & \text{(b)} \end{cases} \tag{2}$$

Where $\boldsymbol{T}(t)$ (dim. N) is the state vector, $\boldsymbol{U}(t)$ (dim. p) contains the thermal inputs and $\boldsymbol{Y}(t)$ (dim. q) the computed outputs that are selected by the user. $\boldsymbol{A}$, $\boldsymbol{B}$, $\boldsymbol{D}$ are respectively the state, input and output matrices.

Moreover, it has been shown how Eqs. (2) could be written under a low dimensioned state-space formulation:

$$\begin{cases} \dot{\boldsymbol{X}}(t) = \boldsymbol{F}\boldsymbol{X}(t) + \boldsymbol{G}\dot{\boldsymbol{U}}(t) & \text{(a)} \\ \boldsymbol{Y}(t) = \boldsymbol{H}\boldsymbol{X}(t) + \boldsymbol{S}\boldsymbol{U}(t) & \text{(b)} \end{cases} \tag{3}$$

Where $\boldsymbol{X}(t)$ (dim. $n \ll N$) is the new state vector in a reduced modal base, $\boldsymbol{F}$ the diagonal matrix of eigenvalues, $\boldsymbol{G}$ and $\boldsymbol{H}$ the input and output matrices and $\boldsymbol{S}$ the static matrix.

In this paper, instead of computing matrices $\boldsymbol{F}$, $\boldsymbol{G}$, $\boldsymbol{H}$ and $\boldsymbol{S}$ from an original DM, they will be identified from experimental data. Then, the formulation of Eqs. (3) ensures us a good model structure in the case of heat diffusion process.

Let us underline that the main advantage of this identification is that the knowledge of thermal properties as well as the heat transfer coefficients (for convective boundary condition) are not necessary. These parameters will be included in the matrices $\boldsymbol{F}$, $\boldsymbol{G}$, $\boldsymbol{H}$ and $\boldsymbol{S}$. IM will then provide a relation between the thermal inputs included in $\boldsymbol{U}(t)$ and the outputs included in $\boldsymbol{Y}(t)$. So, this model gives a Multi-Input Multi-Output (MIMO) relation through a low-order state equation. It is then particularly well adapted to IHCP, which consists

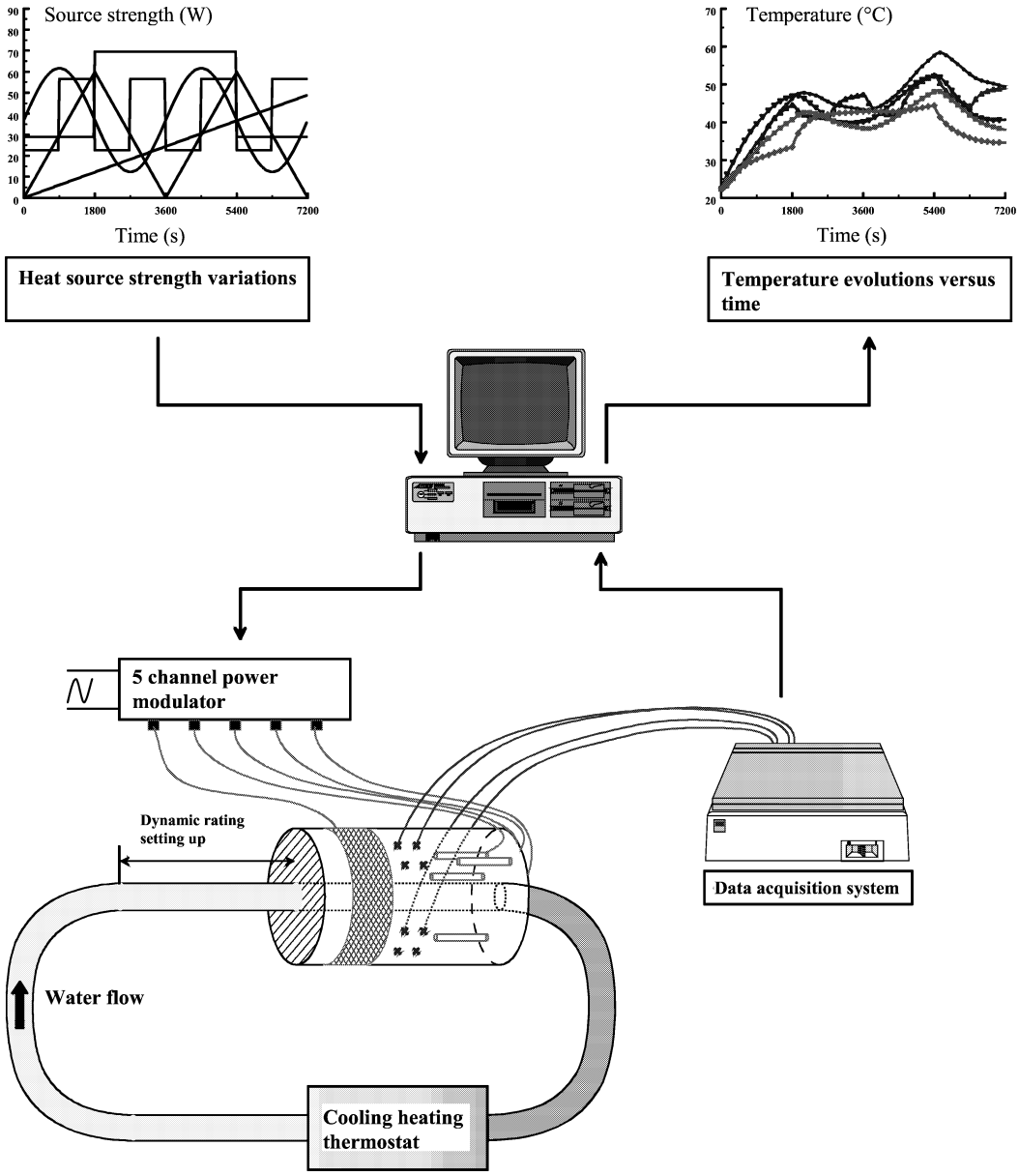

Fig. 2. General view of the device.

in the estimation of the input vector $\boldsymbol{U}(t)$ from the knowledge of $\boldsymbol{Y}(t)$.

The principle of our model identification consists in a minimization procedure of a quadratic criterion built on the difference between the temperature measurements and IM outputs given by Eq. (3b).

It should be noted that several inputs are included in $\boldsymbol{U}(t)$. In order to set up the IM Eqs. (3), several elementary identified models, built on each component of $\boldsymbol{U}$, are used.

3.2. Elementary identified model

As the assumption of linearity is made, the superposition principle can be applied.

In fact, IM is built with as many EIMs as components of $\boldsymbol{U}$: each component $U_i(t)$ is associated with an EIM. Let $u(t) = U_i(t)$ $(1 \leqslant i \leqslant p)$ be the current component of $\boldsymbol{U}$. Each EIM has a similar structure as Eq. (3) and can be written as:

$$\begin{cases} \dot{\boldsymbol{x}}(t) = \boldsymbol{f}\boldsymbol{x}(t) + \boldsymbol{g}\dot{u}(t) & \text{(a)} \\ \boldsymbol{y}(t) = \boldsymbol{h}\boldsymbol{x}(t) + su(t) & \text{(b)} \end{cases} \tag{4}$$

where $\boldsymbol{x}$ (dim. m) is a state vector relative to the scalar u, and $\boldsymbol{f}$ is the corresponding matrix of the eigenvalues f_i $(1 \leqslant i \leqslant m)$. The output vector $\boldsymbol{y}$ represents the contribution of the $u(t)$ effect in the final output vector $\boldsymbol{Y}$ of Eq. (3b).

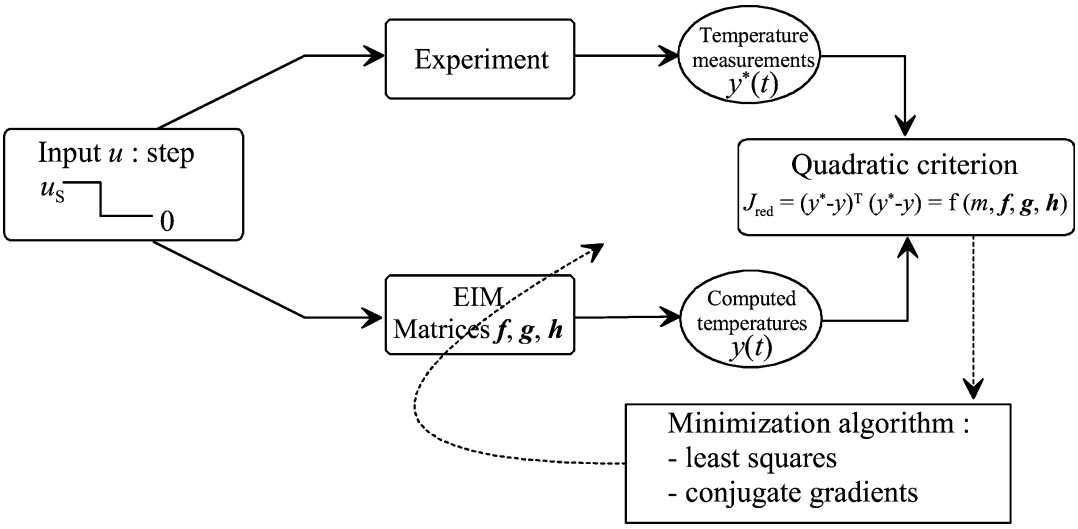

Fig. 3. Principle of experimental modelling.

Note that this formulation also gives information about the time constants τ_i as:

$$f_i = -\frac{1}{\tau_i}, \quad 1 \leqslant i \leqslant m \tag{5}$$

It has been shown [11–14] how all the different matrices in Eqs. (4), as well as the order m, can be obtained with an identification procedure. It consists in the minimization of a quadratic criterion relative to the difference between the experimental outputs $\boldsymbol{y}^*$ (decreasing temperature measurements) and the analytical outputs of EIM $\boldsymbol{y}$ when a step is applied as shown in Fig. 3. For a given order m, this criterion J_{red} is written as:

$$J_{\text{red}}(m, \boldsymbol{f}, \boldsymbol{g}, \boldsymbol{h}) = \sum_{i=1}^{q} \sum_{k=1}^{nt} \left[y_{ik}^*(\text{experiment}) - y_{ik}(\text{EIM}) \right]^2 \tag{6}$$

where nt is the number of time steps contained in the q outputs.

The experimental procedure is then the following one. For each heat source (here VS1, VS2, VS3, VS4 and SS5) and relatively to the $q = 20$ sensors:

- Setting of a constant power on each source independently: $u = u_S = \text{constant}$.
- Storage of the corresponding steady output vector $\boldsymbol{y}_S^*$ for the 20 sensors.
- Calculation of the static vector $\boldsymbol{s}$ from Eq. (4) with $\dot{\boldsymbol{x}}(t) = 0$ and $\dot{u}(t) = 0$. Then, each component of $\boldsymbol{s}$ is approached by:

$$s_i = \frac{(y_s^*)_i}{u_s}, \quad 1 \leqslant i \leqslant q \tag{7}$$

- At $t = 0$, the power is cut off and the temperature decreases are stored (Fig. 4). An exponential time step is used in order to obtain more temperature information at short times.

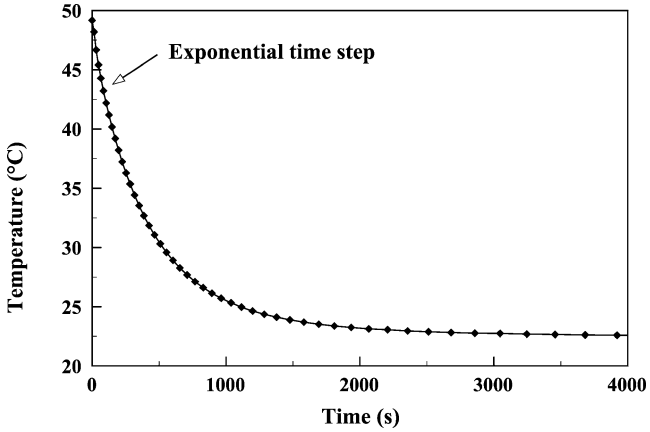

Fig. 4. Decreasing temperature of sensor T1 relatively to SS5.

- Minimization of the quadratic criterion given by Eq. (6) in order to obtain m, $\boldsymbol{f}$, $\boldsymbol{g}$, $\boldsymbol{h}$.

For the 5 sources, the results concerning the time constant values τ_i $(1 \leqslant i \leqslant m)$ are given in Table 2. For each input, we can see that:

- The quadratic criterion J_{red} decreases versus the identified order m.
- The order $m = 10$ corresponds to a stabilization of J_{red}.
- In fact, for $m = 10$, J_{red} $(\approx 0.035\,^\circ\text{C}^2)$ is in relation to the measurement noise.

We have tested several values of m for each EIM. The use of the order $m = 5$ has been chosen for each EIM. The act of increasing m has not significantly improved the direct and inverse computation results.

Note. For each EIM, this identification corresponds to a kind of Duhamel formulation. The responses of step inputs are given through this EIM and only on the measured points.

Table 2
Identified time constants and quadratic criterion J_{red} for each order m of EIM

m		1	2	3	4	5	6	7	8	9	10
source											
VS1	τ (s)	520	540	600	638	1053	1123	1160	1191	1191	1191
			232	151	213	404	409	362	361	430	590
				72.5	117	216	240	360	360	361	430
					31.4	45.1	85.1	186	186	360	362
						44.9	29.7	38.5	119	186	359
							29.6	28.9	38.5	119	186
								28.6	28.9	38.5	119
									28.6	28.9	38.5
										28.6	28.9
											28.6
	J_{red} (°C^2)	28.4	1.87	0.43	0.20	0.075	0.053	0.047	0.046	0.044	0.041
VS2	τ (s)	530	530	632	640	885	2813	4040	4123	4123	4123
			214	138.1	213	356	607	660	664	670	670
				137.9	91.4	216	186.7	219	217.3	217.2	217.2
					22.3	59.9	186.6	218	217.1	217.1	217.1
						24.9	50.5	51.0	51.0	51.0	51.0
							25.1	45.7	45.7	45.7	45.7
								25.1	25.1	39.4	39.4
									20.0	25.1	25.3
										19.9	25.1
											19.9
	J_{red} (°C^2)	42.6	3.65	0.65	0.27	0.082	0.050	0.042	0.041	0.038	0.036
VS3	τ (s)	500	536	604	637	1663	2260	2712	5581	3285	3297
			250	165	226	510	545	582	5574	3280	3295
				60.6	96.5	219	260	221.3	556	527	526
					39.2	53.5	130	221.1	201	258	258
						53.3	43.08	30.9	198	157	157
							43.07	26.8	35.5	83.3	83.3
								26.2	24.4	22.4	42.1
									23.0	21.0	22.4
										18.4	21.0
											18.4
	J_{red} (°C^2)	25.3	2.17	0.39	0.16	0.069	0.050	0.039	0.034	0.032	0.032
VS4	τ (s)	587	564	659	1825	1618	2410	3211	4132	4132	4189
			201	199	484	440	529	2247	4130	4130	4075
				123	187	231	155	526	546	546	546
					94.3	63	155	157.5	179	179	179
						6.8	35.7	157.1	176	177	177
							11.0	31.6	56.7	176	176
								12.3	31.5	56.7	56.7
									12.3	31.5	31.5
										12.3	27.1
											12.3
	J_{red} (°C^2)	16.7	1.50	0.30	0.13	0.066	0.041	0.036	0.033	0.033	0.032
SS5	τ (s)	509	551	636	1271	1538	1681	1682	1636	1636	1639
			197	231	453	487	514	517	493	493	493
				62.6	169	253	267	275	491	491	491
					31.9	29.1	55.8	66.5	255	255	255
						29.0	22.1	31.9	60.8	60.8	60.8
							8.8	13.0	22.3	22.3	22.3
								8.4	14.6	17.4	17.4
									6.7	14.6	15.0
										6.7	14.6
											6.7
	J_{red} (°C^2)	296	26.9	5.94	2.00	0.41	0.062	0.039	0.035	0.034	0.033

3.3. IM reconstitution

When all the p EIMs are identified, IM can be reconstituted from all the p relations (4). The matrices of the complete IM given by Eq. (3) have then the following form:

$$\begin{aligned}
&\boldsymbol{X} = \left[\boldsymbol{x}_1 \cdots \boldsymbol{x}_p\right]^{\mathrm{T}} \\
&\boldsymbol{F} = \left[\mathrm{diag}(\boldsymbol{f}_i)\right], \quad 1 \leqslant i \leqslant p \\
&\boldsymbol{G} = \left[\mathrm{diag}(\boldsymbol{g}_i)\right], \quad 1 \leqslant i \leqslant p \\
&\boldsymbol{H} = [\boldsymbol{h}_1 \cdots \boldsymbol{h}_p] \\
&\boldsymbol{S} = [\boldsymbol{s}_1 \cdots \boldsymbol{s}_p]
\end{aligned} \tag{8}$$

$\boldsymbol{X}$ is then a macro vector, and $\boldsymbol{F}$, $\boldsymbol{G}$, $\boldsymbol{H}$, $\boldsymbol{S}$ macro matrices built with the current elements of Eqs. (4): $\boldsymbol{x}$, $\boldsymbol{f}$, $\boldsymbol{g}$, $\boldsymbol{h}$ and $\boldsymbol{s}$. Each EIM in relation to U_i is characterised by its own order m_i $(= 5)$ and the final IM order will be then:

$$n = \sum_{i=1}^{p} m_i \tag{9}$$

So, here we have $n = 5 \times 5 = 25$. Let us underline that the main advantage of this representation is that each input acts with its own dynamics in relation to the output vector. The inputs have consequently no correlated influences.

For any IM order, matrix $\boldsymbol{S}$ is built with all the vectors $\boldsymbol{s}$ from Eq. (7):

$$\boldsymbol{S} = \begin{array}{c} \\ \mathrm{T1} \\ \mathrm{T2} \\ \mathrm{T3} \\ \mathrm{T4} \\ \mathrm{T5} \\ \mathrm{T6} \\ \mathrm{T7} \\ \mathrm{T8} \\ \mathrm{T9} \\ \mathrm{T10} \\ \mathrm{T11} \\ \mathrm{T12} \\ \mathrm{T13} \\ \mathrm{T14} \\ \mathrm{T15} \\ \mathrm{T16} \\ \mathrm{T17} \\ \mathrm{T18} \\ \mathrm{T19} \\ \mathrm{T20} \end{array} \begin{array}{c} \begin{array}{ccccc} \mathrm{VS1} & \mathrm{VS2} & \mathrm{VS3} & \mathrm{VS4} & \mathrm{SS5} \end{array} \\ \left[\begin{array}{ccccc}
4.73\times10^{-2} & 4.09\times10^{-2} & 2.97\times10^{-2} & 2.86\times10^{-2} & 0.238 \\
3.60\times10^{-2} & 2.96\times10^{-2} & 3.69\times10^{-2} & 3.05\times10^{-2} & 0.242 \\
2.71\times10^{-2} & 3.07\times10^{-2} & 4.27\times10^{-2} & 2.20\times10^{-2} & 0.202 \\
2.63\times10^{-2} & 3.04\times10^{-2} & 2.77\times10^{-2} & 1.64\times10^{-2} & 0.150 \\
0.100 & 7.72\times10^{-2} & 4.07\times10^{-2} & 5.45\times10^{-2} & 0.150 \\
5.36\times10^{-2} & 3.92\times10^{-2} & 5.60\times10^{-2} & 5.14\times10^{-2} & 0.131 \\
4.23\times10^{-2} & 5.38\times10^{-2} & 0.110 & 4.01\times10^{-2} & 0.165 \\
6.54\times10^{-2} & 9.90\times10^{-2} & 6.73\times10^{-2} & 3.53\times10^{-2} & 0.178 \\
0.182 & 0.120 & 5.18\times10^{-2} & 8.71\times10^{-2} & 9.83\times10^{-2} \\
0.120 & 6.77\times10^{-2} & 5.57\times10^{-2} & 9.40\times10^{-2} & 8.48\times10^{-2} \\
7.88\times10^{-2} & 5.12\times10^{-2} & 8.25\times10^{-2} & 8.86\times10^{-2} & 8.58\times10^{-2} \\
6.23\times10^{-2} & 5.77\times10^{-2} & 0.154 & 7.92\times10^{-2} & 0.107 \\
5.47\times10^{-2} & 7.44\times10^{-2} & 0.201 & 5.63\times10^{-2} & 0.106 \\
6.36\times10^{-2} & 0.113 & 0.157 & 4.55\times10^{-2} & 0.112 \\
9.46\times10^{-2} & 0.172 & 9.64\times10^{-2} & 4.75\times10^{-2} & 0.109 \\
0.145 & 0.173 & 6.26\times10^{-2} & 6.14\times10^{-2} & 0.102 \\
0.210 & 9.80\times10^{-2} & 7.37\times10^{-2} & 0.201 & 5.94\times10^{-2} \\
7.98\times10^{-2} & 7.31\times10^{-2} & 0.245 & 0.121 & 7.22\times10^{-2} \\
8.06\times10^{-2} & 0.165 & 0.245 & 5.98\times10^{-2} & 7.59\times10^{-2} \\
0.235 & 0.341 & 8.06\times10^{-2} & 8.58\times10^{-2} & 6.86\times10^{-2}
\end{array}\right] \end{array} \tag{10}$$

Each term $S_{i,j}$ of matrix $\boldsymbol{S}$ represents the static sensitivity of sensor i in relation to input j. Its unit is here $^{\circ}\mathrm{C}\cdot\mathrm{W}^{-1}$. The heat sources are classified as follows: input 1: VS1 in column 1, input 2: VS2 in column 2, etc.

Thanks to this sensitivity matrix, we can notice for example:

- That sensors T5, T9, T10, T16, T17 and T20 are more sensitive to VS1 than other sensors (see column VS1).
- That, for example, sensor T9 is very sensitive to VS1 and VS2.

If these considerations are not very important for the direct simulation, they will have a real interest in the inverse problem, as will be seen further.

3.4. Time discretization

If we assume that $\boldsymbol{U}(t) = \boldsymbol{U}(k+1)$ is constant between time steps $k\Delta t$ and $(k+1)\Delta t$, the time discretization of Eq. (3a) gives (see Appendix A):

$$\boldsymbol{X}(k+1) = \exp[\boldsymbol{F}\Delta t]\left\{\boldsymbol{X}(k) + \boldsymbol{G}\left[\boldsymbol{U}(k+1) - \boldsymbol{U}(k)\right]\right\} \tag{11}$$

Then, Eq. (3b) leads to a linear relation between the output vector $\boldsymbol{Y}(k+1)$ and the input vector $\boldsymbol{U}(k+1)$:

$$\begin{aligned}
\boldsymbol{Y}(k+1) = {} & \left[\boldsymbol{H}\exp(\boldsymbol{F}\Delta t)\boldsymbol{G} + \boldsymbol{S}\right]\boldsymbol{U}(k+1) \\
& + \boldsymbol{H}\exp(\boldsymbol{F}\Delta t)\left[\boldsymbol{X}(k) - \boldsymbol{G}\boldsymbol{U}(k)\right]
\end{aligned} \tag{12}$$

When $\boldsymbol{U}(k)$ is known, Eq. (12) allows the computation of the output vector $\boldsymbol{Y}$ for each time step.

3.5. IM test through a direct problem

Before using IM for the resolution of IHCP, it is necessary to test it. This stage consists in comparing sensor temperatures to the temperatures given by a simulation with IM when all the inputs are known. In the studied case, two heat sources are used: VS2 and SS5. As a result, IM is composed of the two corresponding EIMs of order 5. Fig. 5 shows the strength variations of VS2 and SS5.

The deviation between temperatures simulated with IM and experimental ones is shown in Fig. 6 for two sensors T2 and T20. The quality of these results guarantees that the EIMs are correctly identified.

4. Inverse algorithm

IM is now used in order to solve IHCP. The procedure is sequential. Knowing the input vector $\boldsymbol{U}(k)$ at the time step k, the aim is to estimate the vector $\boldsymbol{U}(k+1)$ from temperatures at time step $k+1$ and/or later. So, future time steps (FTS) [1,3,4] can be used in order to take into account the lagging and damping effects of the diffusion process. A function specification procedure is introduced.

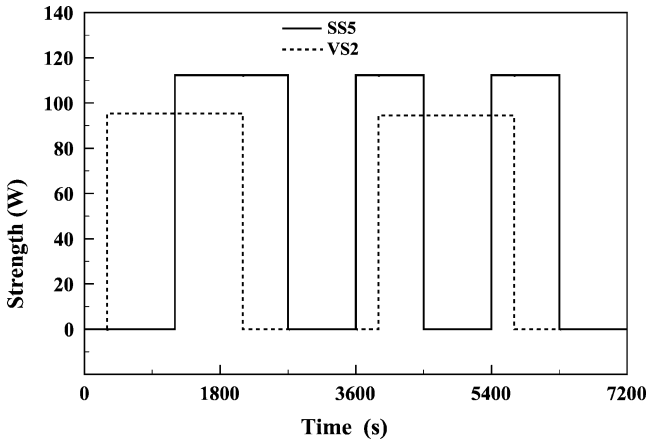

Fig. 5. Strength variations of VS2 and SS5.

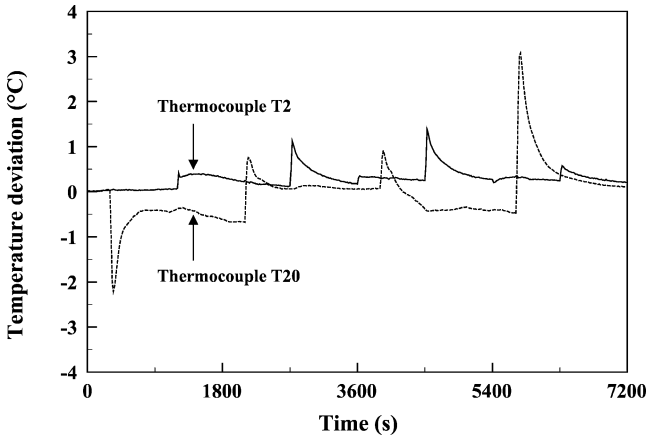

Fig. 6. Deviation between experimental temperatures and computed ones.

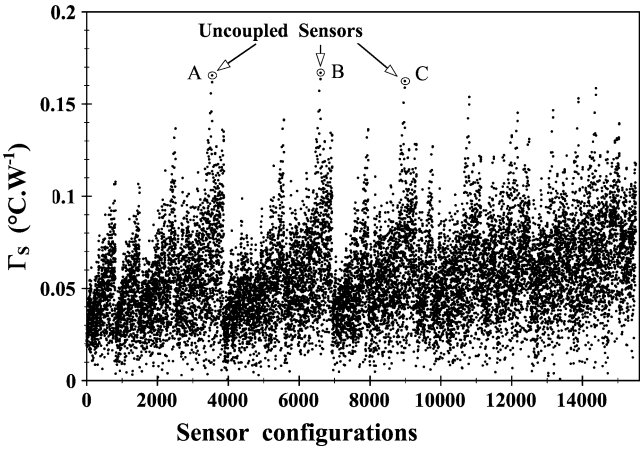

Fig. 7. Decoupling between the sensors.

Consequently, a temporary assumption is made on the additional unknowns: $\boldsymbol{U}(k+1+1),\ldots,\boldsymbol{U}(k+1+nf)$ where nf is the number of FTS. Here, we have chosen:

$$\boldsymbol{U}(k+1+i)=\boldsymbol{U}(k+1) \quad \text{for } 1\leqslant i\leqslant nf$$

According to Eq. (12), the inversion procedure, using the least square method, leads to the resolution of the squared system:

$$\boldsymbol{C}^{\mathrm{T}}\boldsymbol{C}\boldsymbol{U}(k+1)=\boldsymbol{C}^{\mathrm{T}}\big(\boldsymbol{Z}^{*}-\boldsymbol{B}\big) \tag{13}$$

with:

$$\boldsymbol{C}=\begin{bmatrix}\boldsymbol{c}_0\\ \boldsymbol{c}_1\\ \vdots\\ \boldsymbol{c}_{nf}\end{bmatrix}\quad \boldsymbol{B}=\begin{bmatrix}\boldsymbol{b}_0\\ \boldsymbol{b}_1\\ \vdots\\ \boldsymbol{b}_{nf}\end{bmatrix}\quad \boldsymbol{Z}^{*}=\begin{bmatrix}\boldsymbol{Y}^{*}(k+1)\\ \boldsymbol{Y}^{*}(k+1+1)\\ \vdots\\ \boldsymbol{Y}^{*}(k+1+nf)\end{bmatrix} \tag{14}$$

where:

$$\boldsymbol{c}_i=\boldsymbol{H}\exp\big[(i+1)\boldsymbol{F}\Delta t\big]\boldsymbol{G}+\boldsymbol{S} \quad \text{for } 0\leqslant i\leqslant nf \tag{15a}$$

$$\boldsymbol{b}_i=\boldsymbol{H}\exp\big[(i+1)\boldsymbol{F}\Delta t\big]\times\big[\boldsymbol{X}(k)-\boldsymbol{G}\boldsymbol{U}(k)\big] \quad \text{for } 0\leqslant i\leqslant nf \tag{15b}$$

The addition of future time steps takes into account the lagging and damping effects of the diffusion process. Moreover, it is a regularization procedure, which acts directly on the matrix $(\boldsymbol{C}^{\mathrm{T}}\boldsymbol{C})$ to invert (Eq. (13)). This technique is well adapted to the sequential method.

5. Results and discussion

The experimental apparatus is composed of 20 sensors and 5 heat sources. Each source is submitted to various strength variations for two hours (sinusoidal, triangular or square time-varying strength).

Using 20 sensors, temperature histories are measured at different locations in the diffusive medium for two hours with $\Delta t=30$ s.

Many inversion tests have been carried out [11]. For example, the strength variations of the 5 heat sources have been identified from all the 20 temperature evolutions and the identification results were very good because of the overdetermined system.

So, in this paper, we present only the results concerning five sensors that have to be selected among the twenty. That corresponds to $C_{20}^{5}=15\,504$ possibilities. In order to obtain satisfactory inversion results, it is important that the sensors should be uncoupled. This correlation notion can be appreciated with five-order determinants extracted from the sensitivity matrix. So, the 15 504 five-order determinants have been calculated using the static sensitivities of matrix $\boldsymbol{S}$ given by Eq. (10). Let us recall that the matrix $\boldsymbol{S}$ has been previously obtained during the identification process. In order to keep the dimension of sensitivity; we extract the fifth root of the five-order determinants. Consequently, the variable $\Gamma_S=\sqrt[5]{\det(\boldsymbol{S})}$ ($^{\circ}\mathrm{C}\cdot\mathrm{W}^{-1}$) gives the uncorrelation between the sensors.

Of course, to invert, the most favourable case is when the value of Γ_S is maximum. The higher is this value, the better is the configuration. The 15 504 values of Γ_S are shown on Fig. 7. We can see, for example, that configurations A, B and C correspond to relevant choices of sensors for the inversion.

The greatest value of Γ_S ($\Gamma_S=0.167\,^{\circ}\mathrm{C}\cdot\mathrm{W}^{-1}$, configuration B on Fig. 7) corresponds to the sensors T2, T9, T17, T19 and T20. Consequently, this set of sensors is used for the inversion.

Note. It should be noted that the sensors that are the nearest from the sources are T1, T16, T17, T18 and T20. Consequently, the greatest value of Γ_S does not correspond to an obvious configuration where each sensor is located near a source. This can be explained by the fact that the nearest thermocouples are also sensitive to other sources. For example, T1, which is the nearest thermocouple from SS5, is also sensitive to VS1, VS2 and VS4. On the contrary, T2 is further from SS5 but is less sensitive to the volume sources.

The temperature evolutions of these sensors are represented in Fig. 8. The temperature acquisition period is equal

Table 3
Influence of the number of FTS nf on σ_Y

nf	0	1	2	3	4	5
σ_Y (°C)	∞	1.27×10^{-2}	3.53×10^{-2}	6.77×10^{-2}	0.108	0.155

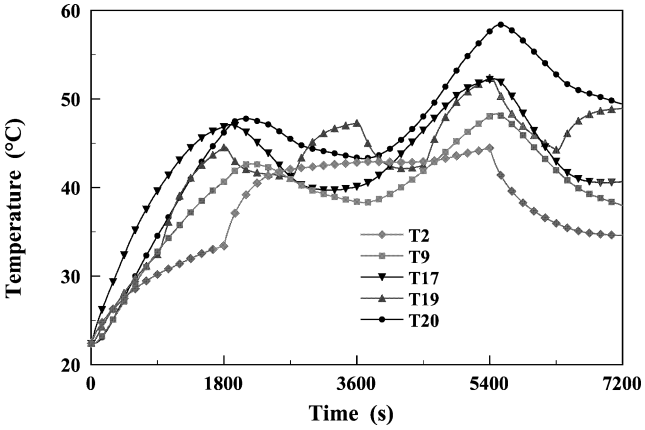

Fig. 8. Temperature evolutions of sensors T2, T9, T17, T19 and T20 with $\Delta t = 30$ s.

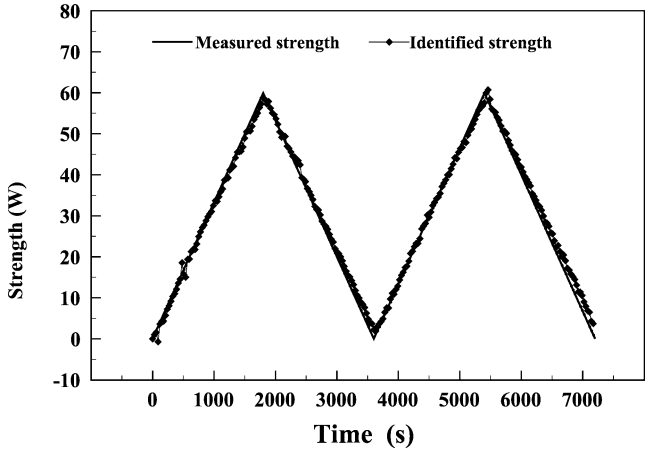

Fig. 9. Estimation of the strength generated by VS1 with $nf = 1$.

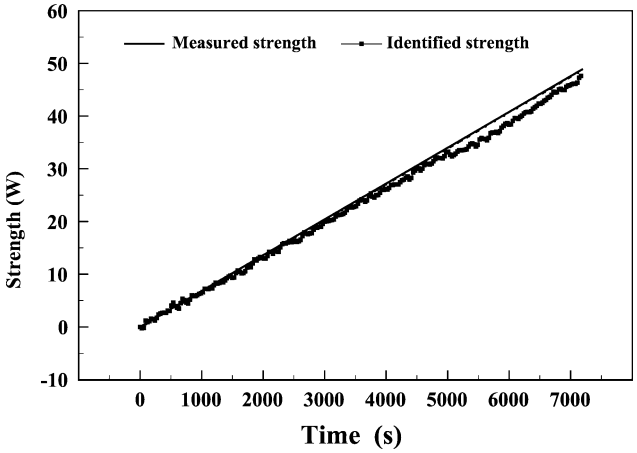

Fig. 10. Estimation of the strength generated by VS2 with $nf = 1$.

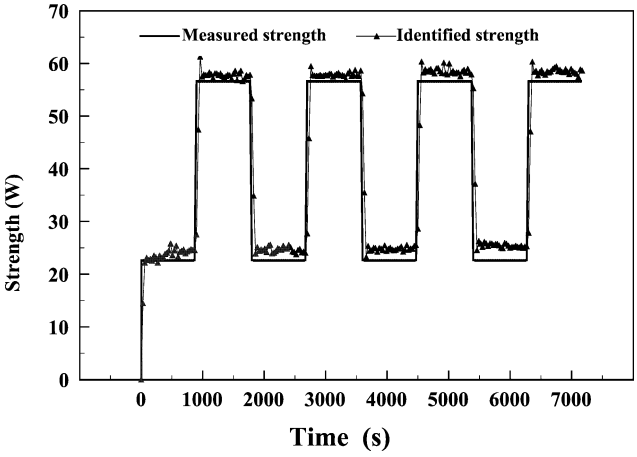

Fig. 11. Estimation of the strength generated by VS3 with $nf = 1$.

to 30 seconds. These temperatures are injected into the inverse algorithm that contains IM composed of 5 EIMs. The resolution of IHCP is done for different numbers of FTS.

For each case, an evaluation of the difference between the original temperatures included in $\boldsymbol{Y}^*$ (the measurements) and the computed ones assembled in $\boldsymbol{Y}$ (calculated with the identified inputs $\boldsymbol{U}$) is calculated. This criterion gives an estimation of the standard deviation of the temperatures and can be written:

$$\sigma_Y = \left[\frac{1}{(nt - 1 - nf) \times q} \times \sum_{i=1}^{q} \sum_{k=1}^{(nt-1-nf)} \left[\boldsymbol{Y}_i^*(k) - \boldsymbol{Y}_i(k) \right]^2 \right]^{1/2} \quad (16)$$

The inversion results are summarised in Table 3 for different nf values. The number of FTS for which σ_Y is the lowest is equal to 1. The optimum value of nf is consequently $nf = 1$.

Remark. This optimum value is in accordance with many references [9,10] where an adimensional time step greater than 0.1 is recommended to solve the IHCP without regularization (for a 2D case). In fact, in our 3D case, using the thermal properties of stainless steel and the sensors and heat sources positions, the different adimensional time steps (relatively to the nearest heat source) can be calculated. They vary between 0.074 and 1.19.

The inversion results, as well as the real strengths, known for this test case (electrically measured) are presented in Figs. 9–13 for each heat source.

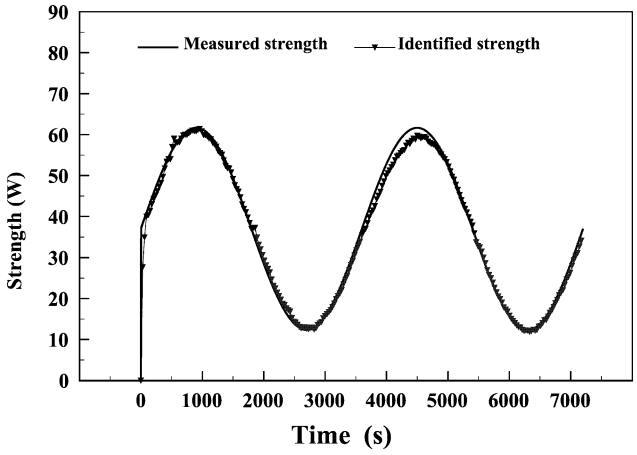

Fig. 12. Estimation of the strength generated by VS4 with $nf = 1$.

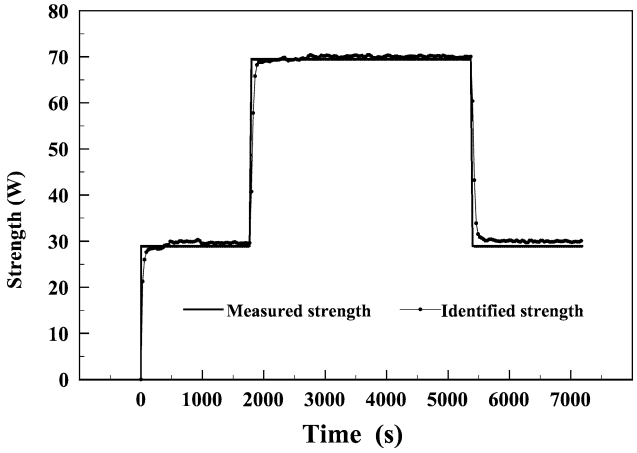

Fig. 13. Estimation of the strength generated by SS5 with $nf = 1$.

Comments

- The results are quite satisfactory except for some small interferences between VS2, VS3 and VS4. The contribution of each heat source to the sensor temperature can be restored, although the strengths vary in very different manners.
- Here, this inversion is carried out with the minimum of sensors ($q = 5$) and the optimum set.
- Nevertheless, the use of other sensors whose sensitivities are more correlated is possible, especially if we use more sensors.
- The computing duration is very small for different reasons:
  - On the one hand, the IM dimension is low and only the computation of a state vector of dimension 25 is needed (included in $\boldsymbol{B}$ Eq. (14)).
  - On the other hand, in the state equation (3a), matrix $\boldsymbol{F}$ is diagonal, thus easy to compute.

6. Conclusion

This study deals with two identification problems that are fundamentally different:

- The first one is related to the model identification knowing its structure and experimental responses to several step excitations. The basic assumptions of this identified model are the linearity and the invariance of parameters.
- The second one consists in using the identified model in order to estimate the strength variations using temperature measurements.

The main advantages of IM are the following:

- Its modal formulation allows to obtain directly and separately the contribution of each heat source to the observed temperatures.
- Its identification is made “in situ”. IM acts as a calibration model including the thermal properties, the convective coefficients, the sensor positions and the contact resistances. The system is modeled in a global way.
- The act of building IM with responses to step inputs integrates weak non-linearities (physical properties, boundary conditions) and then gives a good approximated linear model.
- The computer duration is very low.
- This experimental modelling avoids the spatial discretization of the domain, which leads to a high dimensioned matrix to invert.

All these interesting features have led us to use such a model to invert temperature measurements. This experimental model contains all the parameters of the experiment and restores them in the inverse problem.

Concerning the inverse problem, only the knowledge of a signal proportional to a temperature difference is sufficient in order to identify the thermal strength variations. So, we are not dependent on the accuracy of the sensors: IM acts as a calibration tool for the measurement of the strength generated by heat sources. This methodology could allow the designing of tools for heat flux measurements. Moreover, such an IM could be particularly well adapted for real time process command.

The main drawback lies in the practical realisation of a strength step on each input separately. In industrial context, the thermal systems do not always allow such an approach. Of course, another limit of this approach is that the inversion is made with a model that includes all the thermal properties and boundary conditions. IM is not a parametric model: if a heat transfer coefficient changes, another IM must be identified. However in some cases, by using some correcting fluxes, it is also possible to overcome this difficulty [15].

Appendix A

It is shown that the analytical solution of the state equation:

$$\dot{X}(t) = \boldsymbol{F}X(t) + \boldsymbol{G}\dot{U}(t) \tag{A.1}$$

is given by:

$$X(t) = \mathrm{e}^{\boldsymbol{F}(t-t_0)}X(t_0) + \int_{t_0}^{t} \mathrm{e}^{\boldsymbol{F}(t-\tau)}\boldsymbol{G}\dot{U}(\tau)\,\mathrm{d}\tau$$

We use this analytical solution between $k\times\Delta t$ and $(k+1)\times\Delta t$:

$$X(k+1) = \mathrm{e}^{\boldsymbol{F}\Delta t}X(k) + \int_{k\Delta t}^{(k+1)\Delta t} \mathrm{e}^{\boldsymbol{F}[(k+1)\Delta t-\tau]}\boldsymbol{G}\dot{U}(\tau)\,\mathrm{d}\tau$$

$$X(k+1) = \mathrm{e}^{\boldsymbol{F}\Delta t}X(k) + \mathrm{e}^{\boldsymbol{F}(k+1)\Delta t}\int_{k\Delta t}^{(k+1)\Delta t} \mathrm{e}^{-\boldsymbol{F}\tau}\boldsymbol{G}\dot{U}(\tau)\,\mathrm{d}\tau$$

By integrating the second term by parts:

$$\begin{aligned}
&X(k+1)\\
&\quad= \mathrm{e}^{\boldsymbol{F}\Delta t}X(k) + \mathrm{e}^{\boldsymbol{F}(k+1)\Delta t}\Bigg[\big[\mathrm{e}^{-\boldsymbol{F}\tau}\boldsymbol{G}U(\tau)\big]_{k\Delta t}^{(k+1)\Delta t}\\
&\qquad\qquad + \boldsymbol{F}\int_{k\Delta t}^{(k+1)\Delta t} \mathrm{e}^{-\boldsymbol{F}\tau}\boldsymbol{G}U(\tau)\,\mathrm{d}\tau\Bigg]\\
&\quad= \mathrm{e}^{\boldsymbol{F}\Delta t}X(k) + \mathrm{e}^{\boldsymbol{F}(k+1)\Delta t}\\
&\qquad\times\Bigg[\big[\mathrm{e}^{-\boldsymbol{F}(k+1)\Delta t}\boldsymbol{G}U(k+1) - \mathrm{e}^{-\boldsymbol{F}k\Delta t}\boldsymbol{G}U(k)\big]\\
&\qquad\qquad + \boldsymbol{F}\int_{k\Delta t}^{(k+1)\Delta t} \mathrm{e}^{-\boldsymbol{F}\tau}\boldsymbol{G}U(\tau)\,\mathrm{d}\tau\Bigg]
\end{aligned}$$

By writing that $U(\tau) = U(k+1)$ between time steps $k\times\Delta t$ and $(k+1)\times\Delta t$, we obtain:

$$\begin{aligned}
&X(k+1)\\
&\quad= \mathrm{e}^{F\Delta t}X(k) + \mathrm{e}^{F(k+1)\Delta t}\\
&\qquad\times\Bigg[\big[\mathrm{e}^{-F(k+1)\Delta t}GU(k+1) - \mathrm{e}^{-Fk\Delta t}GU(k)\big]\\
&\qquad\qquad + FGU(k+1)\int_{k\Delta t}^{(k+1)\Delta t} \mathrm{e}^{-Fv}\,\mathrm{d}v\Bigg]\\
&\quad= \mathrm{e}^{\boldsymbol{F}\Delta t}X(k) + \mathrm{e}^{\boldsymbol{F}(k+1)\Delta t}\\
&\qquad\times\big[\big[\mathrm{e}^{-\boldsymbol{F}(k+1)\Delta t}\boldsymbol{G}U(k+1) - \mathrm{e}^{-\boldsymbol{F}k\Delta t}\boldsymbol{G}U(k)\big]\\
&\qquad\qquad - \boldsymbol{G}U(k+1)\big[\mathrm{e}^{-\boldsymbol{F}\tau}\big]_{k\Delta t}^{(k+1)\Delta t}\big]\\
&\quad= \mathrm{e}^{\boldsymbol{F}\Delta t}X(k) + \mathrm{e}^{\boldsymbol{F}(k+1)\Delta t}\\
&\qquad\times\big[\big[\mathrm{e}^{-\boldsymbol{F}(k+1)\Delta t}\boldsymbol{G}U(k+1) - \mathrm{e}^{-\boldsymbol{F}k\Delta t}\boldsymbol{G}U(k)\big]\\
&\qquad\qquad - \boldsymbol{G}U(k+1)\big[\mathrm{e}^{-\boldsymbol{F}(k+1)\Delta t} - \mathrm{e}^{-\boldsymbol{F}k\Delta t}\big]\big]\\
&\quad= \mathrm{e}^{\boldsymbol{F}\Delta t}X(k) + \big[\boldsymbol{G}U(k+1) - \mathrm{e}^{\boldsymbol{F}\Delta t}\boldsymbol{G}U(k)\big]\\
&\qquad - \boldsymbol{G}U(k+1)\big[\boldsymbol{1} - \mathrm{e}^{\boldsymbol{F}\Delta t}\big]
\end{aligned}$$

Finally, the time discretization of Eq. (A.1) is then:

$$X(k+1) = \mathrm{e}^{\boldsymbol{F}\Delta t}X(k) + \mathrm{e}^{\boldsymbol{F}\Delta t}\boldsymbol{G}\big[U(k+1) - U(k)\big]$$

References

[1] J.V. Beck, B. Blackwell, C.R. St. Clair, Inverse Heat Conduction: Ill-Posed Problems, Wiley, New York, 1985, pp. 108–160.

[2] O.M. Alifanov, E.A. Artyukhin, S.V. Rumyantsev, Extreme Methods for Solving Ill Posed Problems with Applications to Inverse Heat Transfer, Begell House, New York, 1995, pp. 152–215.

[3] A.M. Osman, K.J. Dowding, J.V. Beck, Numerical solution of the general two-dimensional inverse heat conduction problem, ASME J. Heat Transfer 119 (1997) 38–45.

[4] J.V. Beck, B. Blackwell, A. Haji-Sheikh, Comparison of some inverse heat conduction methods using experimental data, Internat. J. Heat Mass Transfer 39 (1996) 3649–3657.

[5] Y. Jarny, M.N. Ozisik, J.P. Bardon, A general optimization method using adjoint equation for solving multidimensional inverse heat conduction, Internat. J. Heat Mass Transfer 34 (1991) 2911–2919.

[6] C. Le Niliot, The boundary-element method for the time-varying strength estimation of point heat sources: Application to a two-dimensional diffusion system, Numer. Heat Transfer Part B 33 (1998) 301–321.

[7] R. Pasquetti, C. Le Niliot, Boundary element approach for inverse heat conduction problems: Application to a bidimensional transient numerical experiment, Numer. Heat Transfer Part B 20 (1991) 169–189.

[8] D. Nortershauser, P. Millan, Resolution of a three-dimensional unsteady inverse problem by sequential method using parameter reduction and infrared thermography measurements, Numer. Heat Transfer Part A 37 (2000) 587–611.

[9] M. Raynaud, J.V. Beck, Methodology for comparison of inverse heat conduction methods, ASME J. Heat Transfer 110 (1988) 30–37.

[10] G. Blanc, M. Raynaud, T.H. Chau, A guide for the use of the function specification method for 2D inverse heat conduction problems, Rev. Gén. Therm. 37 (1998) 17–30.

[11] E. Videcoq, Problèmes inverses en diffusion thermique instationnaire: Résolution par représentation d'état et apport de la réduction de modèle, Ph.D. Thesis, Université de Poitiers, 1999.

[12] E. Videcoq, D. Petit, Model reduction for the resolution of multidimensional inverse heat conduction problems, Internat. J. Heat Mass Transfer 44 (10) (2001) 1899–1911.

[13] R. Pasquetti, D. Petit, Analyse modale d'un processus de diffusion thermique: Identification par thermographie infra-rouge, Internat. J. Heat Mass Transfer 31 (1988) 487–496.

[14] D. Petit, R. Hachette, D. Veyret, A modal identification method to reduce a high-order model: Application to heat conduction modelling, Internat. J. Modelling and Simulation 17 (1997) 242–250.

[15] D. Petit, R. Hachette, Model reduction in linear heat conduction: Use of interface fluxes for the numerical coupling, Internat. J. Heat Mass Transfer 41 (1998) 3177–3189.